The Effects of Water on β-D-Xylose Condensation Reactions

Haitao Dong,[†] Mark R. Nimlos,[‡] Michael E. Himmel,[§] David K. Johnson,[§] and Xianghong Qian*,[†]

Department of Mechanical Engineering, Colorado State University, Fort Collins, Colorado 80523, National Bioenergy Center, National Renewable Energy Laboratory, 1617 Cole Boulevard, Golden, Colorado 80401, Chemical and Bioscience Center, National Renewable Energy Laboratory, 1617 Cole Boulevard, Golden, Colorado 80401

Received: March 20, 2009; Revised Manuscript Received: June 11, 2009

Car−Parrinello-based ab initio molecular dynamics simulations (CPMD) combined with metadynamics (MTD) simulations were used to determine the reaction energetics for the β-D-xylose condensation reaction to form β-1,4-linked xylobiose in a dilute acid solution. Protonation of the hydroxyl group on the xylose molecule and the subsequent breaking of the C−O bond were found to be the rate-limiting step during the xylose condensation reaction. Water and water structure was found to play a critical role in these reactions due to the proton's high affinity for water molecules. The reaction free energy and reaction barrier were determined using CPMD−MTD. We found that solvent reorganization due to proton partial desolvation must be taken into account in order to obtain the correct reaction activation energy. Our calculated reaction free energy and reaction activation energy compare well with available experimental results.

I. Introduction

Significant effort has been devoted to the challenges of utilizing lignocellulosic biomass, one of the earth's most abundant natural renewable resources, to produce diverse bioproducts and clean, renewable biofuels.[1–5] Biochemical conversion of lignocellulosic biomass typically includes three steps: pretreatment, enzymatic hydrolysis, and fermentation.[6,7] Dilute acid pretreatment is one of the leading technologies for the hydrolysis and solubilization of hemicelluloses in biomass. During this process, hemicelluloses (mostly xylan) are hydrolyzed to release short chain xylooligomers and monomeric xylose.[7] Furthermore, a small fraction of β-D-glucose is also released from the xyloglucan in hemicellulose and possibly from cellulose. Depending on the severity (temperature, time, and acidity) of the acid pretreatment, some xylose and glucose molecules undergo an undesirable degradation process that lowers the biomass conversion efficiency. 2-Furaldehyde (furfural) and 5-(hydroxymethyl)-2-furaldehyde (HMF) are the major degradation products from xylose and glucose, respectively, in an acidic environment. In addition to furfural, HMF, and other sugar degradation products, the xylose and glucose molecules can react with themselves or each other in an acidic environment to form various disaccharides or even oligomers, particularly at higher initial sugar concentrations. These reactions are termed "reversion reactions."[8] Reversion reactions have been recognized as an important cause of limited sugar yields at high biomass solids loadings (greater than ∼30%) where higher sugar concentrations are encountered. However, increasing biomass solids loading is an important strategy for reducing biomass processing cost. Evidence from both laboratory- and pilot-scale dilute acid pretreatment of biomass indicates that some of these reversion products cannot be easily hydrolyzed and are toxic to the microorganisms used in fermentation.[8,9]

The condensation reaction of the sugar molecules in acidic solution is typically initiated by the protonation of hydroxyl groups on the sugar molecule, as shown in reactions 1 and 2. The equilibrium and reaction rate constants are needed to quantify this reaction. Both constants can be obtained from the reaction free energy and barrier of the free energy surface (FES). The thermodynamic properties of the disaccharide hydrolysis and the reversion condensation reactions have been measured for a number of disaccharides experimentally.[10–15] Moreover, kinetic measurements have been attempted to determine the activation energies and rate constants for these reactions.[16,17] However, it is very difficult to obtain reliable experimental data because the condensation products are often a mixture of disaccharides with similar structures and properties. This situation is further complicated by the degradation reactions of sugar molecules after protonation of the C2−OH on the sugar ring,[18,19] which competes with the condensation reactions.

Ab initio calculations based on accurate electronic structures can provide energetics for chemical reactions. Advances in simulation techniques have also allowed incorporation of accurate electronic structure methods into the framework of molecular dynamics. In particular, the Car−Parrinello molecular dynamics (CPMD) simulation method[20] effectively separates the slow dynamics of nuclei from the fast-moving electrons.[21] Using density functional theory (DFT) and nonlocalized plane wave basis sets, CPMD has been widely used for investigating chemical reactions and biological processes.[22] To investigate and accelerate the reactions and processes with high activation energies, CPMD incorporates metadynamics (MTD), a sampling technique that modifies the FES with history-dependent bias potentials.[23,24] Metadynamics efficiently fills the reactant and product wells on FES, making barrier-crossing events occur at much higher probabilities than in traditional molecular dynamics or Monte Carlo simulation techniques. Applications of MTD include investigating processes such as acid dissociation,[25,26] hydration of ions,[27] adsorption on surfaces,[28] organic compound syntheses,[29–35] proton transfer in membranes,[36] enzyme mech-

* Corresponding author. E-mail: xhqian@engr.colostate.edu.
[†] Colorado State University.
[‡] National Bioenergy Center, National Renewable Energy Laboratory.
[§] Chemical and Bioscience Center, National Renewable Energy Laboratory.

10.1021/jp9025442 CCC: $40.75
Published on Web 07/02/2009

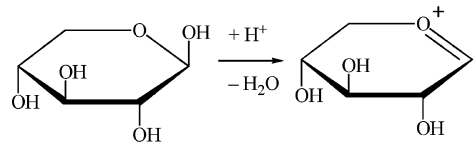

(1)

β-D-xylose

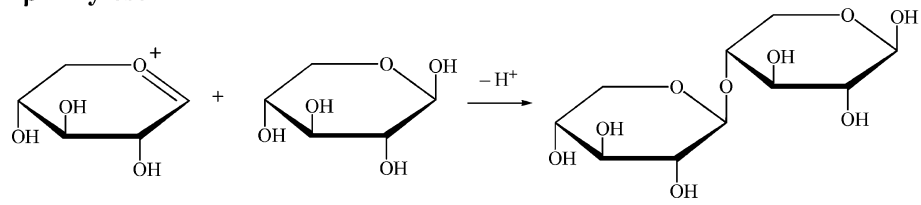

(2)

xylobiose

anisms in large biological systems,[37,38] peptide synthesis,[39,40] and ester hydrolysis.[41] The calculated results obtained using MTD compare satisfactorily with experimental results.

In the present paper, the xylose condensation reaction was investigated using CPMD−MTD simulations. Because protonation and the subsequent breaking of the C−O bond is the crucial rate-limiting step, this work is largely focused on the protonation process of β-D-xylose. The process of transferring a proton from a hydronium ion (H_3O^+) to the hydroxyl group at the C1 carbon on the xylose sugar ring was initially studied in the gas phase. The free energy surface corresponding to the proton transfer and the subsequent C−O bond breaking process was estimated from the history of the bias potentials in the CPMD−MTD simulations. The effect of solvent water on the protonation process was studied by static electronic structure calculations on discrete structures of optimized xylose and protonated water (PW) clusters in the gas phase, and dynamic CPMD−MTD simulations were carried out in bulk water. The gas phase structures were obtained by placing optimized protonated water clusters with one to four water molecules close to the xylose molecule. The structures including the xylose and protonated water clusters were further optimized using Gaussian03. CPMD−MTD was also used to investigate the protonation of the ether linkage in β-1,4-xylobiose in water. β-1,4-Xylobiose is one of the main products of the xylose condensation reaction. Experimental results of this reaction are also available for comparison.[15,17]

II. Methods and Computational Details

A. MTD. MTD is designed to enhance the probabilities of the energy-barrier crossing events during a chemical reaction or process.[23,24] When the energy barrier is more than a few times higher than thermal energy (k_BT), conventional simulation techniques are unable to sample the configurational space that is important to determine the free energy surface. The basic assumption of the MTD method is that FES depends on n ($n \ll 3N$ with N being the number of atoms in the system) collective variables (CVs); here, the ith CV is denoted as S_i. For each CV, an auxiliary particle s_i with fictitious mass m and coupling constant k is coupled to S_i, and the extended Lagrangian of the system becomes

$$L = L_0 + \sum_i m_i \dot{s}_i^2 - \sum_i \frac{1}{2} k_i (S_i - s_i)^2 - V(s) \qquad (3)$$

where L_0 is the original Lagrangian. In this study L_0 is governed by the ab initio CPMD calculations. The second term on the right-hand side is the kinetic energy of the auxiliary particle, s, and the third is the harmonic coupling potential between S and s. The last term represents the history-dependent bias potentials, which are dependent on the dynamics of s. The symbols m and k are the mass and coupling constant for s, respectively. With a proper choice of m and k, the motions of s can be tuned much slower than the motions of S, so it stays at the bottom of the local FES. The derivative of the bias potential, $-\partial V/\partial s$, is added to the equation of motion of s as a time-dependent force component until the system has enough energy to overcome the barrier; for example, a chemical reaction proceeds. Then the product well in turn is filled by the bias potential until another barrier-crossing event occurs. The negative sum of the bias potentials then forms an estimate of the underlying FES. This method is advantageous over the traditional free energy methods, such as the umbrella sampling technique because a good knowledge of FES does not have to be known a priori in MTD sampling.

SCHEME 1: Protonation of C1−OH on Xylose, Reaction

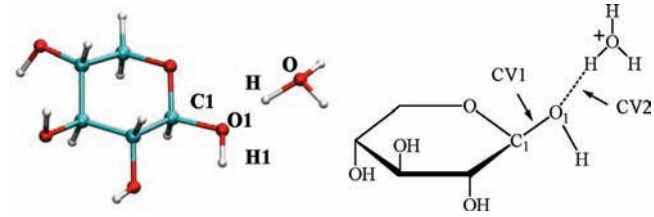

B. MTD Simulation Parameters for Xylose Condensation Reaction. To compute the free energy surface for the formation of xylobiose from xylose, the reaction has been broken down into the two steps shown in reactions 1 and 2. For ease of computation, reaction 2 has been studied in reverse. The selection of the collective variables for the protonation of the C1−OH in xylose (reaction 1) is shown in Scheme 1. The first CV (CV1) is the coordination number (CN) of C1 with respect to O1. The second CV (CV2) is the CN of O1 with respect to proton H. The equation of CN is given by

$$CN = \frac{1 - (d_{ij}/d_0)^p}{1 - (d_{ij}/d_0)^q} \qquad (4)$$

where d_{ij} is the distance between atoms i and j, d_0 is a preset cutoff distance, and the high powers (p and q) distinguish between the coordinated and noncoordinated states. For CV1

SCHEME 2: Protonation of the Ether Linkage in Xylobiose, Reverse of Reaction 2

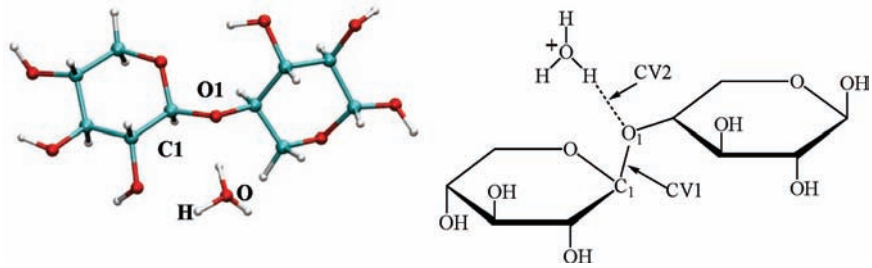

and CV2, the values for d_0 are 1.8 and 1.4 Å, respectively. The values $p = 6$ and $q = 12$ were chosen for both CVs.

Scheme 2 shows the CV setup for the proton transfer from H_3O^+ to the β-1,4-xylobiose linkage. This is the reverse of reaction 2. In this case, the CN parameters were $d_0 = 2.0$ and 1.5 Å for CV1 and CV2, respectively. The values $p = 6$ and $q = 12$ are again chosen for both CVs. The free energy of the complete condensation reaction was obtained by subtracting the free energy change of Scheme 2 from that of Scheme 1.

The dynamics of the fictitious CVs are controlled by the force constant k and mass m (see eq 1). In our simulations, $k = 2.0$ au and $m = 50$ amu were used for both CV's in Scheme 1 We have also tested $k = 8.0$ au and $m = 600$ amu for CV1 and $k = 2.0$ au and $m = 100$ amu for CV2 for a tighter coupling between the real and fictitious variables. The results do not show significant differences. For Scheme 2, we used $k = 8.0$ au and $m = 600$ amu for CV1 and $k = 3.0$ au and $m = 100$ amu for CV2.

The bias potential $V(s)$ used in our metadynamics simulations takes a Gaussian function form,

$$V(s) = \sum_i H \exp\left(-\left(s_i - s_i^0\right)^2/2W^2\right) \qquad (5)$$

Adding a repulsive bias potential will force the system to leave the current location, s^0. The height of the Gaussian, H, is usually a few percent of the reaction barrier.[42,43] The width, W, is preset at a value that is narrower than the mean fluctuations of S. For multidimensional cases in which there is more than one CV, a scaling factor is used for each dimension of W to fit the actual shape of FES in that dimension. Equation 5 can be modified with a second Gaussian to reduce the overlap between successive additions of the bias potentials. However, studies have shown that this second Gaussian does not lead to a significant improvement and, therefore, was not used in our simulations.[37] The height and width of the Gaussian bias potentials were set as $H = 0.001$ au and $W = 0.05$ au. When the first barrier crossing was observed, the value of H was reduced to 0.0005 au and was fixed for the rest of simulations. The bias potentials were added whenever the displacements in the CVs were larger than 1.5 times the width, but no shorter than 100 MD steps. Studies have shown that this choice of parameters is efficient in filling energy wells within an error of 1−2 kcal/mol.[23,43,44]

C. Additional Computational Details. All molecular dynamics calculations were carried out using the CPMD software package. In these CPMD runs, the Becke, Lee, Yang, and Parr (BLYP) functional was used to describe the chemically active valence electrons.[45,46] The interactions between these electrons with the "frozen cores" were described by the Goedecker pseudopotentials.[47] An energy cutoff of 70 Ry was used to for the plane-wave basis sets, which is shown to be sufficient to carry out these calculations from our earlier results.[48] To effectively separate the motions of electrons from those of slow moving nuclei, a fictitious mass of 800 amu and a time step of 0.125 fs were used, as in our earlier calculations.[18,48,49] The MD simulations were carried out under NVT at 300 K with a Nose−Hoover chain thermostat.[50] In the gas phase, the simulation box was decoupled from their images by using the Hockney's method with an extra 4 Å added to each of the dimensions of the simulation box.[51] The simulation box for xylose reaction with a hydronium ion has the dimensions of 13 × 13 × 13 in angstroms. In water, the periodic boundary condition was used for a box containing one xylose, one hydronium ion, one chloride counterion, and 50 water molecules with the box size dimensions of 11.744 × 12.126 × 13.407 in angstroms. Ewald summation was used to integrate the long-range electrostatic interaction energies. An overall water density of 0.94 g/cm^3 was used for the simulation box containing xylose and one proton and counterion, chloride. A total of 68 water molecules were included in the xylobiose simulation box with a corresponding water density of 0.93 g/cm^3 and box size dimensions of 12.568 × 11.514 × 19.251 in angstroms. The Gaussian03 software package was used for the static electronic structure calculations on the gas phase structures involving xylose and protonated water clusters as well as for estimating solvation free energies of the sugar molecules.[52]

III. Results and Discussion

A. Protonation of Xylose C1−OH in the Gas Phase. The protonation of the xylose C1−OH was first studied in the gas phase at 300 K. Figure 1 shows the trajectories of the two CVs during the MTD simulation. Initially, the C1 and O1 are bonded, and therefore, CV1 starts at a value close to 1 (eq 3). CV2 also starts close to 1. Soon after the simulation started, the proton on the hydronium ion was transferred to the O1 of the xylose C1−OH. This process appears to be spontaneous, and there is no barrier associated with it. As studied and suggested earlier

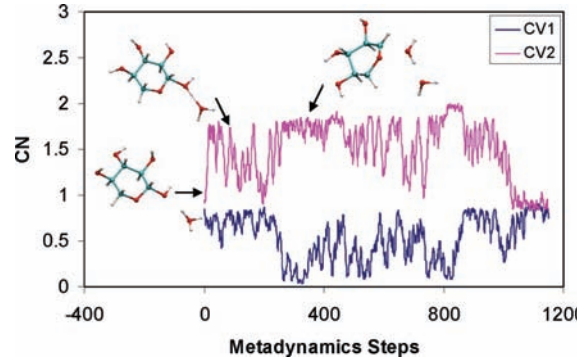

Figure 1. The trajectories of the two collective variables (CV) during MTD simulation for the protonation of C1−OH on xylose in the gas phase at 300 K.

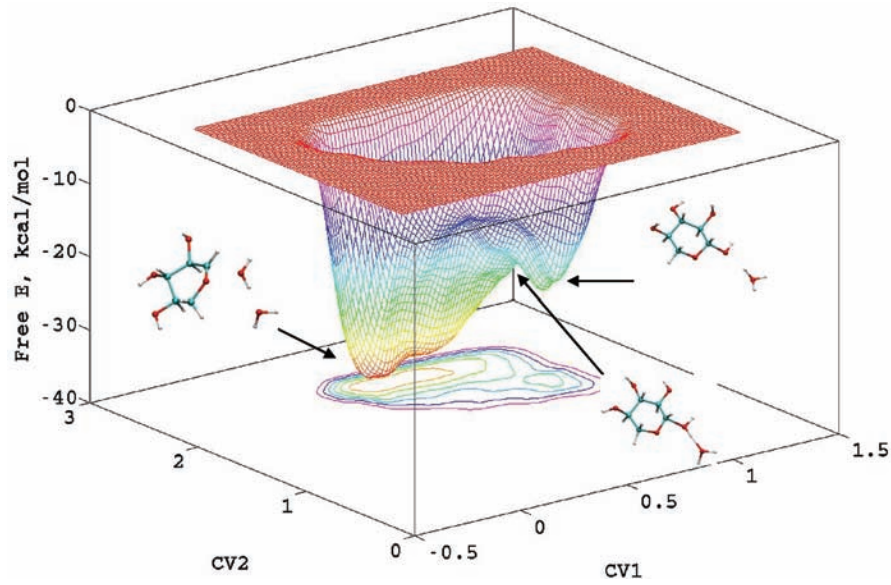

Figure 2. Free energy surface estimated from the MTD simulation for the protonation of the xylose C1−OH and subsequent breaking of the C−O bond (reaction 1) in the gas phase at 300 K.

in literature,[53–57] an isolated hydronium ion is not stable. As a result, the association of the hydronium ion with the −OH groups on the xylose molecule is a spontaneous process with no barrier. Our result agrees with these earlier studies. Following the initial protonation of the C1−OH, the proton is transferred back and forth between C1−OH and H_2O a few times, reflecting the progress of filling the reactant well on FES. At the 240th MTD step, the reactant well appears to be filled, and the system moves to the product well. As shown in Figure 1, CV1 decreases to almost 0 and CV2 increases to around 2. This means that the bond between C1 and the protonated OH group (OH_2) was broken. An oxocarbenium ion and two water molecules were formed (reaction 1).

We found that the filling of the product well on the FES continues after the initial barrier crossing. Figure 1 shows that between the 240th and the 1000th MTD steps, CV1 fluctuates between 0 and 1; and CV2, between 1 and 2. The product well is then filled up by the bias potentials, and the system moves back to the reactant well. The two CVs were shown to be back to their initial values after the 1050th MTD step. This simulation was completed when the system returned to the initial position and both the reactant and product wells were filled.

Figure 2 shows the FES for the xylose protonation reaction in the gas phase at 300 K. This surface is the negative total of the bias potentials added during the simulation. The surface reveals two minima: the first minimum is located at CV1 = 0.8 and CV2 = 1.3, corresponding to the reactant well where the proton stays relatively close to the hydronium ion. The second minimum is at CV1 = 0.2 and CV2 = 1.8, corresponding to the product well where the oxocarbenium ion and two waters are formed following the breaking of C1−O1 bond. The free energy difference between these two minima is −11 kcal/mol, in favor of the products. On the free energy surface, the reaction coordinate (RC) corresponds to the saddle points connecting the two minima. The highest point on the RC indicates the location of the transition state. Figure 2 shows that this transition state is located at CV1 = 0.8 and CV2 = 1.4. In this state, the proton is approximately in the middle position between the two oxygen atoms in water and xylose C1−OH, respectively, whereas the C1−O1 bond remains bonded. This indicates that there is a very small barrier (∼1 kcal/mol) for proton transfer from the water molecule to the xylose C1−OH. This value is only slightly higher than the thermal energy at 300 K, where k_BT = 0.6 kcal/mol. Thermal fluctuation can easily overcome this barrier, particularly at elevated temperatures. The free energy of the protonated xylose is approximately the same as the free energy of the reactant state. Once the xylose C1−OH is protonated, the breaking of C1−O1 appears to be essentially barrierless.

B. Effects of Water on Protonation of Xylose C1−OH. The FES obtained from the CPMD−MTD simulations provides the reaction energetics and reaction coordinate for the protonation of xylose C1−OH. However, the FES obtained with CPMD−MTD describes the interaction energy only when the hydronium ion is in close vicinity to the xylose molecule and the subsequent process of C1−OH protonation and C−O bond breaking. The energy associated with the transport of the hydronium ion to the proximity of the xylose molecule was not taken into account. To quantify the interaction energy as a function of the separation distance between H_3O^+ ion and the xylose molecule, static electronic structure calculations using Gaussion03 were carried out to determine the interaction free energies as a function of the distance between the O atom in xylose C1−OH and the O atom in H_3O^+ in the gas phase at 300 K. These calculations are complementary to the MTD-derived FES, which displays poor sampling of the FES when the O−O distance is longer than 2 Å. The xylose−H_3O^+ complex was first optimized at the B3LYP/6-31+G(d) level, and its free energy was determined using the rigid rotor and harmonic oscillator approximationa. We also calculated the interactions between the xylose and protonated water clusters (PW_n) with n = 1−4, which involves 1, 2, 3, and 4 water molecules, respectively, to explore the effects of water on the free energy of protonation of the xylose C1−OH.

Figure 3a shows the optimized structure of the xylose-PW1 (or hydronium ion) complex. The O1−O distance for the optimized structure is 2.48 Å. Other optimized structures of xylose protonated water clusters with 2, 3, and 4 water molecules are also shown in Figure 3b, c and d, respectively. The equilibrium O1−O bond distance increases as the number of water molecules increases. This result indicates that the interaction between xylose and PW becomes weaker as more water

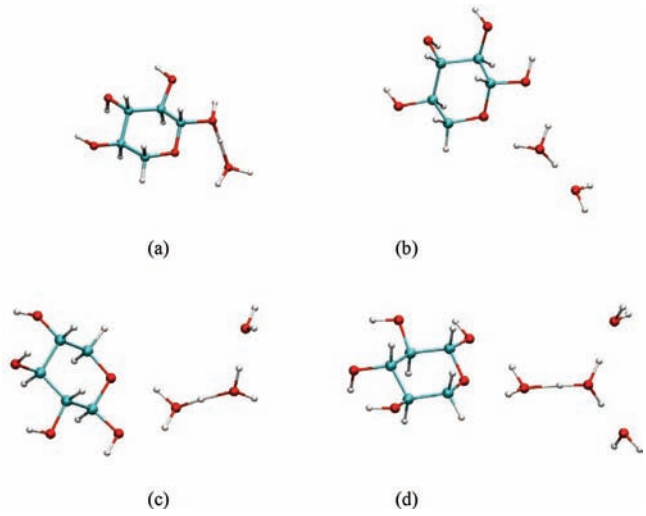

Figure 3. The optimized geometries of (a) xylose−H_3O^+ (protonated water, PW1) complex, (b) xylose−$H_5O_2^+$ (PW2), (c) xylose−$H_7O_3^+$ (PW3), and (d) xylose−$H_9O_4^+$ (PW4).

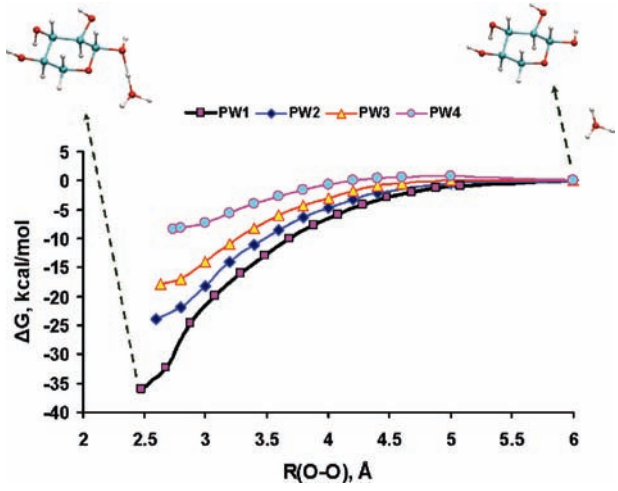

Figure 4. The interaction free energy between xylose and PW clusters as a function of the distance between the O atom in xylose C1−OH.

molecules are associated with the proton. Figure 4 shows the free energy profiles for xylose−PW complexes as a function of the O1−O distance. The maximum O−O distance of 7.0 Å examined is considered to represent complete separation, and the free energies (the sum of the isolated xylose and the isolated PW free energies) are set to zero. Between the completely separated structures and the optimized structures, 10−15 intermediate structures were selected with varying O1−O distances. Their electronic energies were calculated at B3LYP/6-31+G(d), and the entropic contributions were approximated by a linear interpolation between the entropies of the two extreme structures.

The PW1 shows the strongest association with the xylose molecule, with a free energy change of −36.2 kcal/mol and equilibrium O1−O distance of 2.48 Å. The strong interaction between the H_3O^+ and other molecules has been observed and reported previously.[58] However, as the number of water molecules involved in the PW clusters increases, so the association energy between the PW and the xylose molecule weakens. From Figure 4, it can be estimated that the free energy change becomes −25.7, −19.4, and −9.6 kcal/mol for PW2, PW3, and PW4, respectively. This considerable weakening of the interaction between the xylose molecule and the growing PW clusters suggests that water plays an important role in the protonation of the xylose C1−OH. Most likely, protonation of the C1−OH will become increasingly difficult as the number of water molecules associated with the proton increases. We conclude that the stabilization of the proton is probably due to its increased mobility, which leads to an increase in the entropy of the system and is also probably due to the stronger hydrogen bonding interactions resulting from cooperative hydrogen bonding effects.[48] In aqueous solution, the proton affinity of water is expected to be even higher due to the higher number of water molecules associated with the proton. Theoretical investigations have shown that the proton is, indeed, delocalized due to an extensive H-bonding network.[59,60]

C. Protonation of Xylose C1−OH in Water. Figure 5 shows the CPMD−MTD simulation results of the FES for the protonation of xylose C1−OH in water at 300 K. Due to the presence of water, the features of the FES have changed significantly compared to the results in vacuum (Figure 2). Here, reaction 1 is endothermic, whereas in vacuum, the reaction is calculated to be exothermic. In addition, in water solution, there appears to be an additional minimum between the reactants (xylose + hydronium ion) and products (xylose carbocation and two water molecules). In this intermediate structure, the proton has transferred from the solvent to the xylose molecule, but the C1−O1 bond has not broken. The reactant well (corresponding to CV1 = 0.9 and CV2 = 1.1) has a lower free energy with respect to the product well (corresponding to CV1 = 0.1 and CV2 = 1.8). In contrast to the gas phase case, in which the protonation and dehydration decrease the free energy, here the free energy increases by about 6 kcal/mol for proton transfer from the water molecules in solution to C1−OH on xylose. This result clearly shows that the protonation of xylose C1−OH is an unfavorable process in water due to the proton's high affinity for water. Once the C1−OH is protonated, the C−O bond starts to break, and the free energy of the system increases further. The free energy reaches a maximum value at CV1 = 0.4 and CV2 = 1.8 and was found to be 8 kcal/mol higher than the protonated xylose molecule. This position defines the transition state, where the length of the C−O bond is ∼1.8 Å. After passing through the transition state, the free energy of the system decreases by 3 kcal/ mol, and the system reaches the product well. The overall free energy change for protonation of the xylose C1−OH and the subsequent breaking of the C−O bond was found to be 11 kcal/mol, whereas the reaction barrier was found to be 14 kcal/mol.

To validate the free energy result given by CPMD−MTD simulations in water, the reaction free energy was also determined using umbrella sampling. For protonation of the xylose C1−OH, the results using these two methods agree well (see Figure 6a). To compare directly with the umbrella sampling result, the $x-y$ axes of the free energy profile from CPMD−MTD were converted from coordination number type to distance type along the O1−O bond. We found that the differences between MTD and umbrella sampling results were less than 1 kcal/mol. The overall free energy changes for protonation were also within 1 kcal/mol from each other. Figure 6b shows the free energy profiles given by the two methods for the C−O bond-breaking process. The free energies given by MTD were slightly lower than those given by umbrella sampling. The free energy change for breaking the C−O bond using umbrella sampling was found to be about 3 kcal /mol higher than the corresponding MTD result.

Nimlos and co-workers studied the intrinsic kinetics of the glucose condensation reaction in highly agitated microwave-

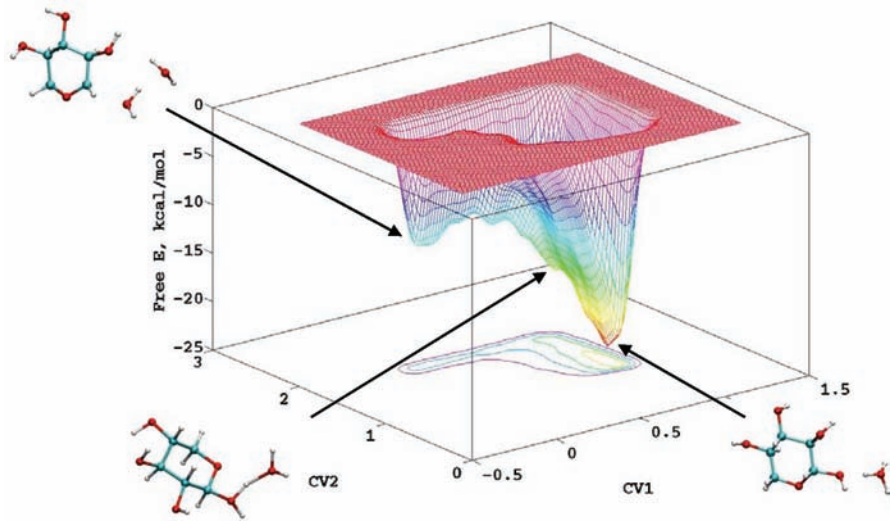

Figure 5. FES for protonation of the xylose C1−OH and the breaking of the C−O bond and the closest O atom in the PW clusters (reaction 1) in water at 300 K using CPMD−MTD simulations.

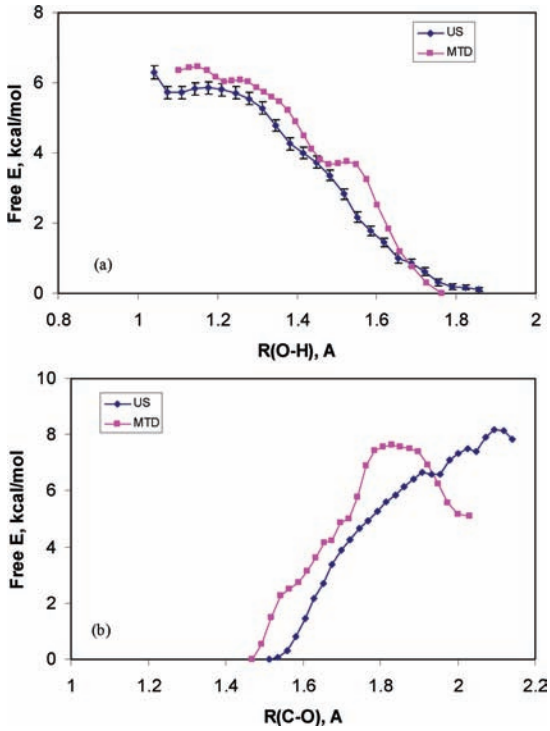

Figure 6. (a) Free energy profiles for the protonation of xylose C1−OH in water at 300 K using CPMD−MTD and umbrella sampling. (b) Free energy profiles for the breaking of the C1−O bond using CPMD−MTD and umbrella sampling in water at 300 K.

heated reaction vessels.[17] An activation barrier of 27 kcal/mol for the reaction was found. One might expect a similar reaction barrier for xylose, but our calculated activation energy of 14 kcal/mol is significantly lower than this. Note that the estimated error involved in CPMD−MTD free energy calculations is only about 2−3 kcal/mol. This large difference must come from processes that are not included in the CPMD−MTD simulations. In fact, the xylose molecule and H_3O^+ are already in close proximity in the starting geometry of the simulation. The free energy contribution from solvent reorganization that involves moving the proton in the bulk water to the neighborhood of the xylose molecule is not accounted for in our CPMD−MTD simulations. We studied the free energy change of this proton's partial desolvation process by employing a thermodynamic cycle

SCHEME 3: Thermodynamic Cycle for Determining the Free Energy Change of Proton Partial Desolvation Process

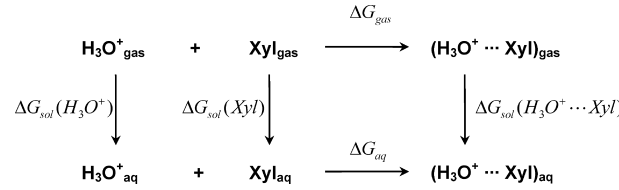

(Scheme 3). The free energy of proton partial desolvation, ΔG_{aq}, can be determined by calculating the gas phase free energy change, ΔG_{gas}, and the solvation free energies, ΔG_{sol}, of both the reactants and products. The free energy changes in both the gas phase and water were calculated as a function of the distance between the H_3O^+ ion and the xylose molecule. Gaussion03 was used in the calculations. Since static Gaussian calculations as a function of distance cannot reproduce the dynamic proton movement process, the calculated results are only an approximation to the actual proton partial desolvation process.

Polarizable continuum models (PCM) have been used to calculate solvation free energies for neutral molecules and ions in many different types of solvents.[61] Although the explicit solvent structures are overlooked in these models, the outcome of the calculations has been satisfactory. In this study, we use the conductor-like PCM (CPCM), which has given accurate solvation free energies for organic acids to determine the solvation free energy of the xylose−H_3O^+ complex.[62–64] In addition to the gas phase free energies for moving the hydronium ion toward the xylose, the solvation contributions to the free energies of those structures were calculated to give the total free energies in water. The solvation free energies were calculated with PBE0 on the DFT-derived structures and with UAKS atomic radii, which are developed specifically for the PBE0 method.[65] This method gives a solvation free energy of −105.4 kcal/mol for the hydronium ion. Considering the small size and large charge of H_3O^+, this result agrees reasonably well with the experiment value of −110 kcal/mol. The errors in free energy differences are expected to be less due to systematic error cancellation.

Figure 7 shows the solvation free energies of the xylose−H_3O^+ structures with the O1−O distance varying from 2.48 to 7.0 Å. The gas phase free energies of the same structures

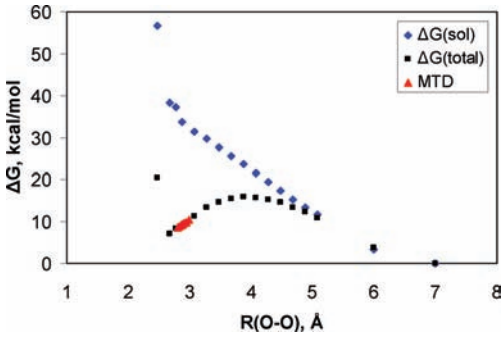

Figure 7. Solvation free energy (Δ*G* (sol)) and partial desolvation free energy (Δ*G* (total)) for moving H_3O^+ close to the xylose molecule with an O1−O distance varying from 2.48 to 7.0 Å. The red triangles correspond to the free energies for the distances derived from CPMD−MTD simulations.

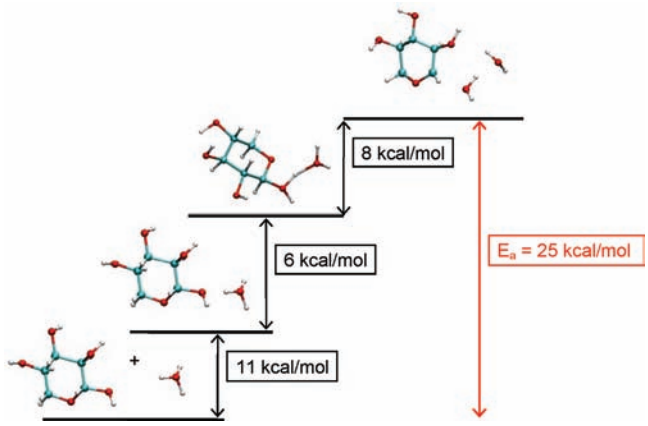

Figure 8. Free energy profile for protonation of xylose C1−OH and the subsequent breaking of the C−O bond (energies are not to scale).

are presented in Figure 4. The solvation free energies were found to increase as the hydronium ion moves closer to the xylose molecule. The overall free energy change of this partial desolvation process is also plotted in Figure 7. As the O1−O distance decreases, the partial desovlation free energy increases and reaches a maximum of 16 kcal/mol at 3.88 Å. It then decreases to 7 kcal/mol when the O1−O distance reaches 2.68 Å and then increases again rapidly to about 20 kcal/mol for the gas phase optimized structure with an O1−O distance of 2.48 Å. Structures of the xylose−H_3O^+ complexes with such short O1−O distances were not observed in our CPMD−MTD simulations. Figure 7 also shows the O1−O distances of the xylose−H_3O^+ structures corresponding to the free energy minimum on the FES (Figure 5) with CPMD−MTD simulations. The O1−O distance during CPMD−MTD simulations varies between 2.8 and 3.0 Å with a corresponding partial desolvation free energy of 9−11 kcal/mol. This amount of free energy should be added to the total activation energy for the protonation of C1−OH on xylose. The free energy profile combining the CPMD−MTD simulations and the partial proton desolvation process is shown in Figure 8. The total activation energy is therefore around 25 kcal/mol from our calculations, which is in turn in good agreement with experiment.

D. Protonation of the Ether Linkage in β-1,4-Xylobiose. Figure 9 shows the FES from CPMD−MTD simulations of protonation of the ether linkage on β-1,4-xylobiose in aqueous solution at 300 K. This protonation process is similar to the previous case. The two CVs chosen for the simulations are defined earlier in Scheme 2. The FES shows two energy minima. The first is located at CV1 = 0.9 and CV2 = 0.1, corresponding to the reactant state in which the proton remains close to the H_2O molecule. The second minimum is located at CV1 = 0.1 and CV2 = 0.8, corresponding to the product well where the proton has been transferred to the ether linkage and the C1−O1 bond is broken. The overall free energy change is 7 kcal/mol. The transition state is located at CV1 = 0.8 and CV2 = 0.8, with a free energy barrier of 10 kcal/mol over the reactant state. This activation energy is less than the activation energy for protonation of the xylose C1−OH.

The activation energy should once again include the contribution from moving the fully solvated proton from a position in the bulk water phase to a position close to the ether linkage of the xylobiose during CPMD−MTD simulations. Figure 10 shows the solvation free energies and the total free energies for the proton partial desolvation process. The gas phase and solvation free energies were all given by the HF/6-31+G(d) and the UAHF atomic radii.[66] The energy profiles show a trend similar to the earlier case. The free energy for partial proton desolvation reaches a maximum of 21 kcal/mol at a O1−O distance of 3.6 Å. It then decreases to 14 kcal/mol at a O1−O distance of 2.8 Å. The O1−O distances obtained from CPMD−MTD simulations at the bottom of the reactant well are also shown in Figure 10. The proton partial desolvation free energy of ∼15 kcal/mol must be added to the activation energy obtained from CPMD−MTD simulations (see Figure 11). The total activation energy for protonation of the ether linkage and the breaking of the C−O bond during xylobiose hydrolysis is about 25 kcal/mol. Experimental measurements have shown that the activation energies for hydrolysis of disaccharides are about 30 kcal/mol. However, if the maximum partial desolvation free energy is used instead of the value corresponding to CPMD−MTD distances, the estimated activation energy is about 31 kcal/mol, which is in good agreement with experimental measurement.

E. Free Energy for Xylose Condensation Reaction. By subtracting the free energy for the xylobiose reaction (reaction 1) from the free energy of the xylose reaction (reaction 2), the net free energy obtained corresponds to the xylose condensation reaction to form xylobiose. Starting with a xylose molecule and a H_3O^+ ion in solution, the free energy change for proton transfer from H_3O^+ to the xylose C1−OH is 6 kcal/mol. The protonated hydroxyl group then needs to overcome an energy barrier of 8 kcal/mol to break the C−O bond. After the breaking of the C−O bond, the free energy decreases by about 3 kcal/mol to form the intermediate oxocarbenium ion. The second half of the condensation reaction starts with a C−O bond formation between the oxocarbenium ion and C4−OH on another xylose molecule. This process requires about 3 kcal/mol to overcome the barrier. The C−O bond is then formed, and the proton returns to the water molecule. This reaction is associated with 10 kcal/mol of free energy decrease. The overall free energy change for the xylose condensation reaction to form β-1,4 linked xylobiose is 4 kcal/mol. Conversely, the free energy change for the hydrolysis reaction of xylobiose to form two xylose molecules will be about −4 kcal/mol. The free energy landscape of the reactions is schematically shown below in Figure 12.

By using equilibrium and calorimetric measurements, Goldberg and co-workers reported a free energy difference of −4.34 ± 0.06 kcal/mol for the hydrolysis of xylobiose in water at 300 K15. Our calculated value is in very good agreement with these experimental data, considering that the errors involved in free energy calculations are about 2 kcal/mol. The standard enthalpy given by the same experimental work was 0.029 ± 0.062 kcal/

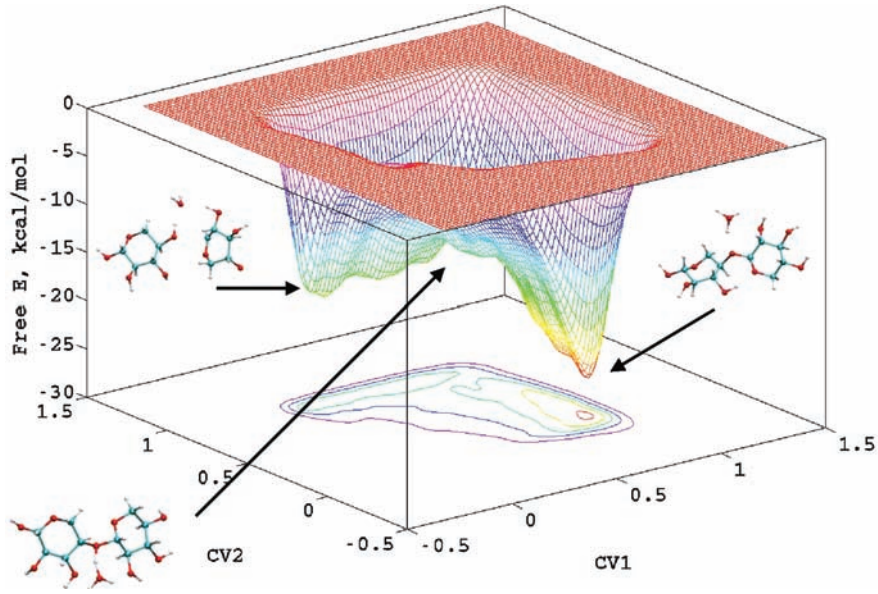

Figure 9. Free energy surface for protonation of the ether linkage in xylobiose and the subsequent breaking of the C−O bond (reaction 2) in water at 300 K from CPMD−MTD simulations.

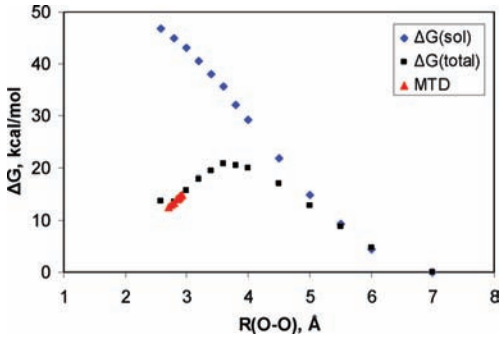

Figure 10. Solvation free energy (ΔG (sol)) and total free energy (ΔG (total)) for the proton partial desolvation process for moving H_3O^+ in bulk water to close to xylobiose with an O1−O distance varying from 7.0 to 2.6 Å. The red triangles correspond to the free energies for the O1−O distances of the reactant well during CPMD−MTD simulations.

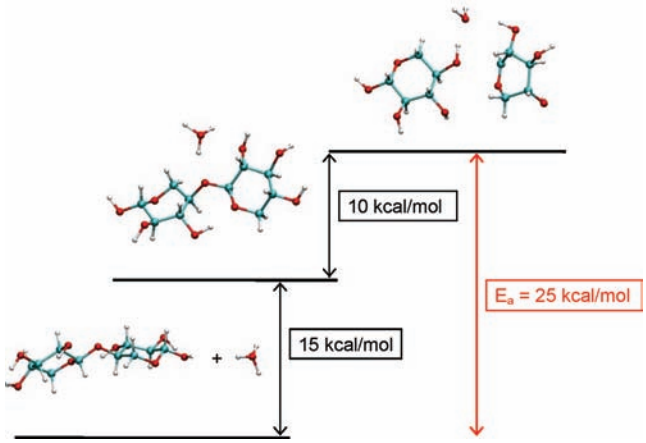

Figure 11. Free energy profile for protonation of the ether linkage on xylobiose and the subsequent breaking of the C−O bond (energies are not to scale).

mol for the hydrolysis reaction. This indicates that this reaction is mainly entropy-driven.

F. Uncertainties. In CPMD−MTD simulations, the FES is estimated by the total bias potentials. The uncertainties associated with this method are dependent on the specific system as well as the parameters that control the progress of adding the bias potentials. Laio and co-workers suggested that when the system's relaxation time and temperature are fixed, the accuracy of the method is an explicit function of the energy well depth, the space of the collective variables, the shape and frequency of the updating Gaussian bias potentials, and the total simulation steps.[43] Using this formula, the uncertainties in the total bias potentials of our simulations were estimated to be 2.0 kcal/mol. This is in the typical range of uncertainties reported in other CPMD−MTD studies. Other errors may lie in the DFT method of the electronic structure calculations, the pseudopotentials for the core−valence electron interactions, and the finite size of basis wave functions. We did not attempt to quantitatively determine these errors, but they should be in the same range as the errors in MTD simulations.

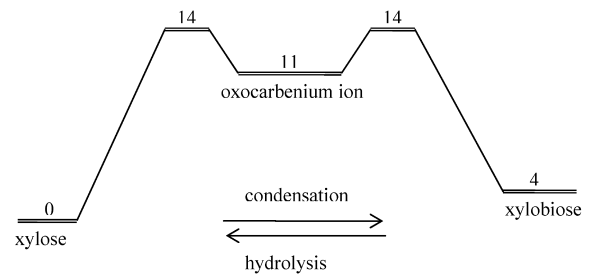

Figure 12. Free energy changes (in kcal/mol) for the hydrolysis or condensation reactions in water at 300 K given by CPMD−MTD simulations.

IV. Conclusions

CPMD−MTD simulations have been used to determine the free energy surface for the xylose condensation reaction. It appears that protonation of the xylose C1−OH and the subsequent breaking of the C−O bond is the rate-limiting step. We found that water and water structure play an important role in the protonation process due to the strong affinity of the solvent water with the proton. The more water molecules associated with the proton, the more delocalized the proton is and the higher the reaction barrier for protonation of the xylose molecule. Further, proton partial desolvation or solvent reorganization free

energy has to be taken into account to get the correct activation barrier. A proton in bulk water and a proton in close proximity to the xylose molecule have different free energies. Our targeted proton resides in close proximity to the xylose molecule during the CPMD−MTD simulations. We further utilized the notion that proton partial desolvation free energy can be determined using static ab initio calculations. Our calculated reaction free energy and reaction barrier compare well with experimental data.

Acknowledgment. This work is supported by the Department of Energy Office of the Biomass Program via a Subcontract from the National Renewable Energy Laboratory (ZCO-7-77386-01). The authors thank Robert N. Goldberg, Bernd Ensing, and Nisanth Nair for helpful discussions. Calculations were carried out using the computing facilities at Colorado State University, National Renewable Energy Laboratory, and Teragrid.

References and Notes

(1) http://www1.eere.energy.gov/biomass/, 2008.
(2) *Polysaccharides. Structural Diversity and Functional Versatility*; Dumitriu, S., Ed.; Marcel Dekker, Inc.: New York, 1998.
(3) Farrell, A. E.; Plevin, R. J.; Turner, B. T.; Jones, A. D.; O'Hare, M.; Kammen, D. M. *Science* **2006**, *311*, 506.
(4) Himmel, M. E.; Ding, S. Y.; Johnson, D. K.; Adney, W. S.; Nimlos, M. R.; Brady, J. W.; Foust, T. D. *Science* **2007**, *315*, 804.
(5) Lynd, L. R.; Cushman, J. H.; Nichols, R. J.; Wyman, C. E. *Science* **1991**, *251*, 1318.
(6) Mosier, N.; Wyman, C.; Dale, B.; Elander, R.; Lee, Y. Y.; Holtzapple, M.; Ladisch, M. *Bioresour. Technol.* **2005**, *96*, 673.
(7) Schell, D. J.; Farmer, J.; Newman, M.; McMillan, J. D. *Appl. Biochem. Biotechnol.* **2003**, *105*−*108*, 69.
(8) Minor, J. L. *J. Appl. Polym. Sci.: Appl. Polym. Symp.* **1983**, *37*, 617.
(9) Nimlos, M. R. Private communication.
(10) Goldberg, R. N.; Bell, D.; Tewari, Y. B.; McLaughlin, M. A. *Biophys. Chem.* **1991**, *40*, 69.
(11) Goldberg, R. N.; Tewari, Y. B. *J. Biol. Chem.* **1989**, *264*, 9897.
(12) Goldberg, R. N.; Tewari, Y. B.; Ahluwalia, J. C. *J. Biol. Chem.* **1989**, *264*, 9901.
(13) Tewari, Y. B.; Goldberg, R. N. *J. Biol. Chem.* **1989**, *264*, 3966.
(14) Tewari, Y. B.; Goldberg, R. N. *Biophys. Chem.* **1991**, *40*, 59.
(15) Tewari, Y. B.; Lang, B. E.; Decker, S. R.; Goldberg, R. N. *J. Chem. Thermodyn.* **2008**, *40*, 1517.
(16) Capon, B. *Chem. Rev.* **1969**, *69*, 407.
(17) Nimlos, M. R.
(18) Qian, X. H.; Nimlos, M. R.; Davis, M.; Johnson, D. K.; Himmel, M. E. *Carbohydr. Res.* **2005**, *340*, 2319.
(19) Qian, X.; Nimlos, M. R. Mechanisms of Xylose and Xylooligomer Degradation During Acid Pretreatment. In *Biomass Recalcitrance*; Himmel, M., Ed.; Blackwell Publishing Ltd: Oxford, 2007; pp in press.
(20) *CPMD3.11*; copyrighted jointly by IBM Corp and by Max-Planck Institute, Stuttgart.
(21) Car, R.; Parrinello, M. *Phys. Rev. Lett.* **1985**, *55*, 2471.
(22) *Ab-initio Molecular Dynamics: Theory and Implementation*; Marx, D., Hutter, J., Eds.; Forschungzentrum Juelich, NIC Series; John von Neumann Institute for Computing: Juelich, 2000; Vol. 1.
(23) Iannuzzi, M.; Laio, A.; Parrinello, M. *Phys. Rev. Lett.* **2003**, *90*, 238302.
(24) Laio, A.; Parrinello, M. *Proc. Natl. Acad. Sci. U.S.A.* **2002**, *99*, 12562.
(25) Lee, J. G.; Asciutto, E.; Babin, V.; Sagui, C.; Darden, T.; Roland, C. *J. Phys. Chem. B* **2006**, *110*, 2325.
(26) Park, J. M.; Laio, A.; Iannuzzi, M.; Parrinello, M. *J. Am. Chem. Soc.* **2006**, *128*, 11318.
(27) Ikeda, T.; Hirata, M.; Kimura, T. *J. Chem. Phys.* **2005**, *122*, 244507.
(28) Rodriguez-Fortea, A.; Iannuzzi, M.; Parrinello, M. *J. Phys. Chem. C* **2007**, *111*, 2251.
(29) Asciutto, E.; Sagui, C. *J. Phys. Chem. A* **2005**, *109*, 7682.
(30) Boero, M.; Ikeshoji, T.; Liew, C. C.; Terakura, K.; Parrinello, M. *J. Am. Chem. Soc.* **2004**, *126*, 6280.
(31) Boero, M.; Tateno, M.; Terakura, K.; Oshiyama, A. *J. Chem. Theory Comput.* **2005**, *1*, 925.
(32) Ensing, B.; Klein, M. L. *Proc. Natl. Acad. Sci. U.S.A.* **2005**, *102*, 6755.
(33) Ensing, B.; Laio, A.; Gervasio, F. L.; Parrinello, M.; Klein, M. L. *J. Am. Chem. Soc.* **2004**, *126*, 9492.
(34) Stirling, A.; Iannuzzi, M.; Parrinello, M.; Molnar, F.; Bernhart, V.; Luinstra, G. A. *Organometallics* **2005**, *24*, 2533.
(35) Zipoli, F.; Bernasconi, M.; Laio, A. *ChemPhysChem* **2005**, *6*, 1772.
(36) Iannuzzi, M.; Parrinello, M. *Phys. Rev. Lett.* **2004**, *93*, 025901.
(37) Babin, V.; Roland, C. *J. Chem. Phys.* **2006**, *125*, 204909.
(38) Boero, M.; Ikeda, T.; Ito, E.; Terakura, K. *J. Am. Chem. Soc.* **2006**, *126*, 16798.
(39) Nair, N. N.; Schreiner, E.; Marx, D. *J. Am. Chem. Soc.* **2008**, *130*, 14148.
(40) Schreiner, E.; Nair, N. N.; Marx, D. *J. Am. Chem. Soc.* **2008**, *130*, 2768.
(41) Gunaydin, H.; Houk, K. N. *J. Am. Chem. Soc.* **2008**, *130*, 15232.
(42) Ensing, B.; Laio, A.; Parrinello, M.; Klein, M. L. *J. Phys. Chem. B* **2005**, *109*, 6676.
(43) Laio, A.; Rodriguez-Fortea, A.; Gervasio, F. L.; Ceccarelli, M.; Parrinello, M. *J. Phys. Chem. B* **2005**, *109*, 6714.
(44) Ensing, B.; De Vivo, M.; Liu, Z.; Moore, P.; Klein, M. L. *Acc. Chem. Res.* **2006**, *39*, 73.
(45) Becke, A. D. *Phys. Rev. A* **1988**, *38*, 3098.
(46) Lee, C.; Yang, W.; Parr, R. G. *Phys. Rev. B* **1988**, *37*, 785.
(47) Goedecker, S.; Teter, M.; Hutter, J. *Phys. Rev. B* **1996**, *54*, 1703.
(48) Qian, X. H. *Mol. Simul.* **2008**, *34*, 183.
(49) Qian, X. H.; Ding, S. Y.; Nimlos, M. R.; Johnson, D. K.; Himmel, M. E. *Macromolecules* **2005**, *38*, 10580.
(50) Nose, S. *J. Chem. Phys.* **1984**, *81*, 511.
(51) Hockney, R. W. *Methods Comput. Phys.* **1970**, *9*, 136.
(52) Frisch, M. J.; Trucks, G. W.; Schlegel, H. B.; Scuseria, G. E.; Robb, M. A.; Cheeseman, J. R.; Montgomery, J. A., Jr.; Vreven, T.; Kudin, K. N.; Burant, J. C.; Millam, J. M.; Iyengar, S. S.; Tomasi, J.; Barone, V.; Mennucci, B.; Cossi, M.; Scalmani, G.; Rega, N.; Petersson, G. A.; Nakatsuji, H.; Hada, M.; Ehara, M.; Toyota, K.; Fukuda, R.; Hasegawa, J.; Ishida, M.; Nakajima, T.; Honda, Y.; Kitao, O.; Nakai, H.; Klene, M.; Li, X.; Knox, J. E.; Hratchian, H. P.; Cross, J. B.; Bakken, V.; Adamo, C.; Jaramillo, J.; Gomperts, R.; Stratmann, R. E.; Yazyev, O.; Austin, A. J.; Cammi, R.; Pomelli, C.; Ochterski, J. W.; Ayala, P. Y.; Morokuma, K.; Voth, G. A.; Salvador, P.; Dannenberg, J. J.; Zakrzewski, V. G.; Dapprich, S.; Daniels, A. D.; Strain, M. C.; Farkas, O.; Malick, D. K.; Rabuck, A. D.; Raghavachari, K.; Foresman, J. B.; Ortiz, J. V.; Cui, Q.; Baboul, A. G.; Clifford, S.; Cioslowski, J.; Stefanov, B. B.; Liu, G.; Liashenko, A.; Piskorz, P.; Komaromi, I.; Martin, R. L.; Fox, D. J.; Keith, T.; Al-Laham, M. A.; Peng, C. Y.; Nanayakkara, A.; Challacombe, M.; Gill, P. M. W.; Johnson, B.; Chen, W.; Wong, M. W.; Gonzalez, C.; Pople, J. A. *Gaussian 03, Revision C.02*; Gaussian, Inc.: Wallingford CT, 2004.
(53) Larson, J. W.; McMahon, T. B. *J. Am. Chem. Soc.* **1986**, *108*, 1719.
(54) Mackay, G. I.; Tanner, S. D.; Hopkinson, A. C.; Bohme, D. K. *Can. J. Chem.* **1979**, *57*, 1518.
(55) Marx, D.; Tuckerman, M. E.; Hutter, J.; Parrinello, M. *Nature* **1999**, *397*, 601.
(56) Mauro Boero, T. I. K. T. *ChemPhysChem* **2005**, *6*, 1775.
(57) Dominik, M. *ChemPhysChem* **2006**, *7*, 1848.
(58) Tortonda, F. R.; Pascual-Ahuir, J.; Silla, E.; Tunon, I. *J. Phys. Chem.* **1995**, *99*, 12525.
(59) Lobaugh, J.; Voth, G. A. *J. Chem. Phys.* **1996**, *104*, 2056.
(60) Schmitt, U. W.; Voth, G. A. *J. Chem. Phys.* **1999**, *111*, 9361.
(61) Tomasi, J.; Mennucci, B.; Cammi, R. *Chem. Rev.* **2005**, *105*, 2999.
(62) Barone, V.; Cossi, M. *J. Phys. Chem. A* **1998**, *102*, 1995.
(63) Dong, H.; Du, H.; Qian, X. *J. Phys. Chem. A* **2008**, *112*, 12687.
(64) Toth, A. M.; Liptak, M. D.; Phillips, D. L.; Shields, G. C. *J. Chem. Phys.* **2001**, *114*, 4595.
(65) Adamo, C.; Barone, V. *J. Chem. Phys.* **1999**, *110*, 6158.
(66) Barone, V.; Cossi, M.; Tomasi, J. *J. Chem. Phys.* **1997**, *107*, 3210.

JP9025442